Electronic Supplementary Material (ESI) for Physical Chemistry Chemical Physics.

Anapole-excited Terahertz Multifunctional Spoof Surface Plasmon Polariton Directional Janus Metastructures

Hao Pan, Bingxiang Li, and Hai-feng Zhang**

1. Electromagnetic multipole expansion

The exterior field can induce the oscillating charges ρ and current density **J** in the metastructure, whose far-field response is equal to the superposition of the electric/magnetic/toroidal multipoles' responses. Therefore, the resonances of metastructures can be equivalent to the composite scattering of multipoles from the perspective of multipole radiation, thus achieving the quantitative analysis of the corresponding resonances, which can contribute to the investigation of the operating mechanism.

For different types of multipoles, the far-field scattering is characterized by a composite forcing of the multipole arrays and is therefore radiated to the far field as a plane wave. The charge density ρ or current density **J** can be used to calculate the multipole moment scattering energy inside the unit structure. In the case of vertical plane wave incidence, each unitary structure can be considered to be excited in the same phase. The multipole array jurisdiction field calculated at a point in the far field can be considered as the sum of the far fields obtained from the scattering of a certain type of multipole excited by the unitary structure in the arrangement. By using electromagnetic simulation software, the charge density or current density excited in the electromagnetic super dielectric can be calculated and thus used to calculate the scattering energy including the conventional electric multipoles, magnetic multipoles, new electric toroidal multipoles, and magnetic toroidal multipoles.

The expressions we have used to calculate the multipole moments from the current density distribution are those given by Radescu and Vaman [1]. Cartesian multipoles are computed by integrating over the charge density $\rho(\mathbf{r})$ or current density $\mathbf{J}(\mathbf{r})$ distribution within the unit cell (α, β, γ=x, y, z) [2],[3]:

$$\mathbf{P} = \frac{1}{i\omega}\int \mathbf{J} d^3 r \tag{S1}$$

$$\mathbf{M} = \frac{1}{2c}\int [\mathbf{r} \times \mathbf{J}] d^3 r \tag{S2}$$

$$\mathbf{M}^{(1)} = \frac{1}{2c}\int \left[\mathbf{r}\times\mathbf{J}\right] r^2 d^3r \tag{S3}$$

$$\mathbf{T} = \frac{1}{10c}\int \left[(\mathbf{r}\cdot\mathbf{J})\mathbf{r} - 2r^2\mathbf{J} \right] d^3r \tag{S4}$$

$$T_\alpha^{(1)} = \frac{1}{28c}\int \left[3r^2 J_\alpha - 2r_\alpha (\mathbf{r}\cdot\mathbf{J}) \right] r^2\, d^3r \tag{S5}$$

$$Q^e_{\alpha,\beta} = \frac{1}{2i\omega}\int [r_\alpha J_\beta + r_\beta J_\alpha - \frac{2}{3}\delta_{\alpha,\beta}(\mathbf{r}\cdot\mathbf{J})]\, d^3r \tag{S6}$$

$$Q^m_{\alpha,\beta} = \frac{1}{3c}\int [(\mathbf{r}\cdot\mathbf{J})_\alpha r_\beta]\, d^3r + \{\alpha \leftrightarrow \beta\} \tag{S7}$$

$$Q^T_{\alpha,\beta} = \frac{1}{28c}\int [4r_\alpha J_\beta(\mathbf{r}\cdot\mathbf{J}) - 5r^2(r_\alpha J_\beta + r_\beta J_\alpha) - 2r^2\delta_{\alpha,\beta}(\mathbf{r}\cdot\mathbf{J})]\, d^3r \tag{S8}$$

$$O^e_{\alpha,\beta,\gamma} = \frac{1}{i6\omega}\int \left[J_\alpha \left(\frac{r_\beta r_\gamma}{3} - \frac{1}{5}r^2\delta_{\beta,\gamma} \right) + r_\alpha \left(\frac{J_\beta r_\gamma}{3} + \frac{J_\gamma r_\beta}{3} - \frac{2}{5}(\mathbf{r}\cdot\mathbf{J})\delta_{\beta,\gamma} \right) \right] d^3r + \{\alpha \leftrightarrow \beta,\gamma\} + \{\alpha \leftrightarrow \gamma,\beta\} \tag{S9}$$

$$O^m_{\alpha,\beta,\gamma} = \frac{15}{2c}\int \left(r_\alpha r_\beta - \frac{r^2}{5}\delta_{\alpha,\beta} \right) (\mathbf{r}\times\mathbf{J})_\gamma\, d^3r + \{\alpha \leftrightarrow \beta,\gamma\} + \{\alpha \leftrightarrow \gamma,\beta\} \tag{S10}$$

The symbols **P**, **M**, **T**, $\mathbf{Q^e}$, $\mathbf{Q^m}$, $\mathbf{Q^T}$, $\mathbf{O^e}$, and $\mathbf{O^m}$ represent electric dipole, magnetic dipole, toroidal dipole, electric quadrupole, magnetic quadrupole, and toroidal quadrupole, electric octupole, and magnetic octupoles, respectively. $\mathbf{M^{(1)}}$ and $\mathbf{T^{(1)}}$ are the magnetic and toroidal mean radius, respectively. For quadrupoles and octupoles, a shorthand has been used to improve clarity. For example,

$$\int \left[(\mathbf{r}\cdot\mathbf{J})_\alpha r_\beta \right] d^3r + \{\alpha \leftrightarrow \beta\} \equiv \int \left[(\mathbf{r}\cdot\mathbf{J})_\alpha r_\beta \right] d^3r + \int \left[(\mathbf{r}\cdot\mathbf{J})_\beta r_\alpha \right] d^3r \tag{S11}$$

And $\{\alpha\leftrightarrow\beta, \gamma\}$ means that the second term is obtained from the first term by exchanging α and β while leaving γ untouched.

All mean radius multipoles appear as a result of the series expansion of the spherical Bessel functions, which are a partial solution of vector/scalar Helmholtz equation in spherical coordinates. The relative strength of the excited multipole moments in a toroidal multipole

metastructure leads to different far-field responses. In general, the scattering power of multipole moment mainly depends on the corresponding power equation of the respective multipole moment, while the overall far-field response is assessed by the total radiated power I_s. The total radiated power I_s of the metastructure is expanded to the fifth order of 1/C in the case of harmonic excitation exp($i\omega t$), as.shown in Equation (S12)

$$I_s = \frac{2\omega^4}{3c^3}|\mathbf{P}|^2 + \frac{2\omega^4}{3c^3}|\mathbf{M}|^2 + \frac{4\omega^5}{3c^4}(\mathbf{P}\cdot\mathbf{T}) + \frac{2\omega^6}{3c^5}|\mathbf{T}|^2 + \frac{\omega^6}{5c^5}\sum\left|Q^e_{\alpha,\beta}\right|^2 + \frac{\omega^6}{40c^5}\sum\left|Q^m_{\alpha,\beta}\right|^2 + O\left(\frac{1}{c^5}\right) \tag{S12}$$

Meanwhile, the far-field scattering $\mathbf{E_s}$ resulting from the multipole moments can be obtained according to the formula:

$$\begin{aligned}\mathbf{E}_s = \frac{\mu_0 c^2}{2\Delta^2}\{&-ik\mathbf{P}_{\parallel} + ik\mathbf{R}\times\left(\mathbf{M}_{\parallel} - \frac{k^2}{10}\mathbf{M}^{(1)}_{\parallel}\right) - k^2\left(\mathbf{T}_{\parallel} + \frac{k^2}{10}\mathbf{T}^{(1)}_{\parallel}\right) + k^2(\mathbf{Q^e}\cdot\mathbf{R})_{\parallel} \\ &- \frac{k^2}{2}\mathbf{R}\times(\mathbf{Q^m}\cdot\mathbf{R})_{\parallel} - \frac{ik^3}{3}(\mathbf{Q^T}\cdot\mathbf{R})_{\parallel} + ik^3[(\mathbf{Q^e}\cdot\mathbf{R})\mathbf{R}]_{\parallel} - \frac{ik^3}{180}\mathbf{R}[(\mathbf{Q^m}\cdot\mathbf{R})\mathbf{R}]_{\parallel}\}\times\exp(-ikR)\end{aligned} \tag{S13}$$

where Δ is the area of the unit cell in the metastructure, R is the distance between the observation plane and the structure surface, and || indicates the parallel components.

2. Radiation of elementary anapole mode

In our discussion, following Afanasiev and Stepanovsky [3], the distribution of radiated electric-magnetic field (**E** and **H**), as well as the scalar φ and vector potential **A** resulting from the electric and toroidal dipole moments can be given by the Equation (S14-S21).

For electric dipole $\mathbf{P}(t) = \mathbf{P}e^{i\omega t}$:

$$\varphi_P = \frac{(\mathbf{r}\cdot\mathbf{P})D(\omega,r)}{cr}\frac{\exp(-ikr+i\omega t)}{r} \tag{S14}$$

$$\mathbf{A}_P = ik\mathbf{P}\frac{\exp(-ikr+i\omega t)}{r} \tag{S15}$$

$$\mathbf{E}_P = \left[\frac{(\mathbf{r}\cdot\mathbf{P})F(\omega,r)}{c^2 r^2}\mathbf{r} - \frac{G(\omega,r)}{c^2}\mathbf{P} \right] \frac{\exp(-ikr + i\omega t)}{r} \tag{S16}$$

$$\mathbf{H}_P = -\frac{ikD(\omega,r)}{cr}[\mathbf{r}\times\mathbf{P}]\frac{\exp(-ikr + i\omega t)}{r} \tag{S17}$$

For toroidal dipole $\mathbf{T}(t) = \mathbf{T}e^{i\omega t}$:

$$\varphi_T = 0 \tag{S18}$$

$$\mathbf{A}_T = \left[\frac{(\mathbf{r}\cdot\mathbf{T})F(\omega,r)}{c^2 r^2}\mathbf{r} - \frac{G(\omega,r)}{c^2}\mathbf{T} \right] \frac{\exp(-ikr + i\omega t)}{r} \tag{S19}$$

$$\mathbf{E}_T = \left[\frac{ikG(\omega,r)}{c^2}\mathbf{T} - \frac{ik(\mathbf{r}\cdot\mathbf{T})F(\omega,r)}{c^2 r^2}\mathbf{r} \right] \frac{\exp(-ikr + i\omega t)}{r} \tag{S20}$$

$$\mathbf{H}_T = -\frac{k^2 D(\omega,r)}{cr}[\mathbf{r}\times\mathbf{T}]\frac{\exp(-ikr + i\omega t)}{r} \tag{S21}$$

In the above cases, the following functions are used to simplify the expression of electric and magnetic fields resulting from electric **P** and toroidal **T** dipole moments:

$$D(\omega,r) = i\omega + \frac{c}{r} = c\left(ik + \frac{1}{r} \right) \tag{S22}$$

$$F(\omega,r) = -\omega^2 + \frac{i3c\omega}{r} + \frac{3c^2}{r^2} = c^2\left(-k^2 + \frac{i3k}{r} + \frac{3}{r^2} \right) \tag{S23}$$

$$G(\omega,r) = -\omega^2 + \frac{ic\omega}{r} + \frac{c^2}{r^2} = c^2\left(-k^2 + \frac{ik}{r} + \frac{1}{r^2} \right) \tag{S24}$$

Based on the superposition of electric and toroidal dipole moments **P** and **T** proposed in this paper, namely the anapole mode, the total electric field $\mathbf{E}_{\mathbf{total}}$ and magnetic field $\mathbf{H}_{\mathbf{total}}$ can be given by

$$\mathbf{E}_{\mathbf{total}}(t) = \left[\frac{F(\omega,r)\mathbf{r}\cdot(\mathbf{P} - ik\mathbf{T})}{c^2 r^2}\mathbf{r} - \frac{G(\omega,r)}{c^2}(\mathbf{P} - ik\mathbf{T}) \right] \frac{\exp(-ikr + i\omega t)}{r} \tag{S25}$$

$$\mathbf{H}_{\mathbf{total}}(t) = -\frac{ikD(\omega,r)}{cr}[\mathbf{r}\times(\mathbf{P} - ik\mathbf{T})]\frac{\exp(-ikr + i\omega t)}{r} \tag{S26}$$

Note that the fields of the anapole disappear in the case of **P** = *ik***T**; i.e., the destructive interference of toroidal and electric dipole moments takes place everywhere except $r = 0$. This configuration forms a nonradiating point anapole, with the fields existing only at the point $r = 0$, and described by the δ function

$$\mathbf{E}_{\mathbf{total}(r=0)} = ik\mathbf{T}\delta(\mathbf{r})\exp(i\omega t) \tag{S27}$$

$$\mathbf{H}_{\mathbf{total}(r=0)} = ik\,\mathrm{rot}\left[\mathbf{T}\delta(\mathbf{r})\right]\exp(i\omega t) \tag{S28}$$

3. Extraction details of mode volume

Mode volume V_m can then be evaluated from the commonly used definition (where ε is the dielectric constant)[4]

$$V_m = \frac{\int \varepsilon |E(r)|^2 dV}{\max\left[\varepsilon |E(r)|^2\right]} \tag{S29}$$

where $\mathbf{E}(r)$ is the electric field. The electric field $\mathbf{E}(r)$ can be obtained from the software HFSS, and the mode volume can be calculated according to Equation (S29). According to the calculated result, the mode volume of anapole-excited metastructure is 4.1×10^{-5} $(\lambda/n)^3$ where λ and n define the wavelength of incident light in free space and refractive index

4. Dephasing time fitting and FDTD simulation

A damped harmonic oscillator model was employed to analytically reproduce the time-resolved photoemission signals employing the dephasing time as the only adjustable parameter [5],[6]. The electric field can be expressed by

$$E(t) \propto \int_{-\infty}^{t} K(t')e^{-\gamma(t-t')}\sin\left[\omega_0(t-t')\right]dt' \tag{S30}$$

where $K(t)$ denotes the driving force and can be expressed as the sum of pump and probe pulses $K(t)=K(t)+K(t+t_d)$, t_d is the delay time between pump and probe pulses. ω_0 denotes

plasmon resonance frequency, and γ=1/2T, where T represents the dephasing time of the plasmon field.

Considering the multiphoton process of photoemission, the time-resolved photoemission intensity can be expressed as

$$I(t_{\mathrm{d}}) \propto \int_{-\infty}^{+\infty} \left|E(t)\right|^{2N} dt \tag{S25}$$

where N denotes the nonlinear order of photoemission. By comparing with the simulation signals for FDTD, the best value of the fitted dephasing time can be obtained.

The properties of such structure excited by anapole mode were simulated using the finite-difference time-domain (FDTD) method (Lumerical FDTD solutions). As shown in Fig.S1, the dephasing time of the anapole-excited metastructure is calculated as 1.43 ps at 2.17 THz.

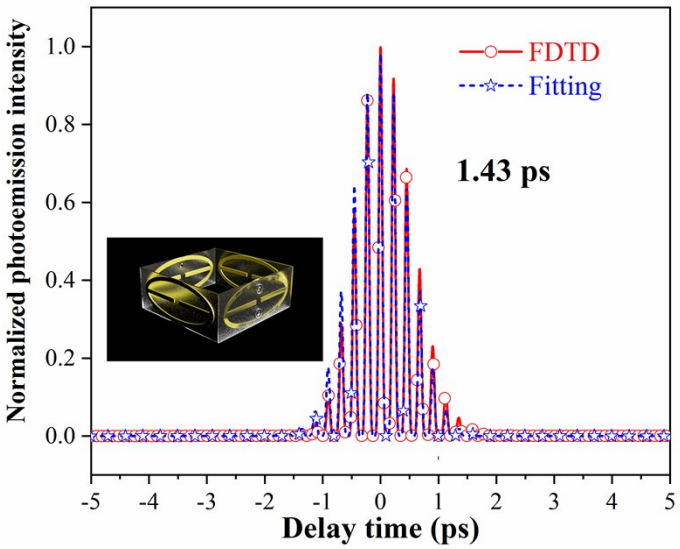

Fig.S1. Normalized photoemission intensity calculated from the electric fields obtained in the finite-difference time-domain (FDTD) simulation and numerically fitted by plasmon oscillator model for the anapole-excited metastructure.

5. Polarization selectivity of MSR

As the forward EM wave is normally incident with different polarization angles, the absorption and co-polarized transmission windows of the MSR consisting of AE SSPP always keep stable, as shown in Fig.S2, signifying that the proposed metastructure is insensitive to the

polarization state, which can be contributed to the symmetry configuration along the propagation. Regardless of the polarization-angle variation of the forward normally incident wave in the absorption band, the electric field vector can always be decomposed into double orthogonal components $\mathbf{E_x}$ and $\mathbf{E_y}$ each parallel to the *x*- and *y*-directions, thus inducing the anapole modes residing in the metallic elliptical rings along the *x*- and *y*-directions, respectively, to greatly improve the EM energy density in the metadevice and then acquire the high absorption independent of the polarization angle. Similarly, the vertical-incident wave with different polarization angles in the transmission window can also be divided into two components transmitting through the gaps between the adjacent rings along the *x*- and *y*-directions, respectively, consequently acquiring the polarization-insensitive transmission window.

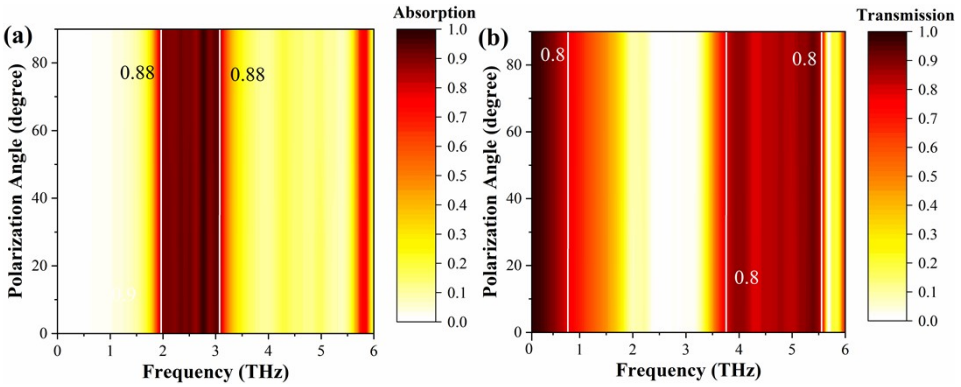

Fig.S2. The EM responses of the unidirectional MSR based on the gradient AE SSPP for the forward incident TE wave with different polarization angles. (a) The absorption versus different polarization angles. (b) The transmission versus different polarization angles.

6. Parameter analysis of multifunctional JMS

The distance *h* between the AE MSR and PCS is a crucial parameter that controls the effect of the field-localization property of anapole mode supported by the bottom elliptical ring on the reflection and absorption of the incident wave. It can be observed in Fig.S3 that with the increase of *h*, the influence of anapole resonance on the backward incident wave is weakened, further resulting in the enhancement of the cross-polarized reflection. In addition, the absorption of the multifunctional JMS for the forward incident wave is first enhanced and then decreased,

which is mainly because of the coupling variation between the MSR and PCS. Considering the comprehensive effect on different functionalities of the proposed JMS for the forward and backward incident waves, the optimized distance *h* is selected as 25 μm.

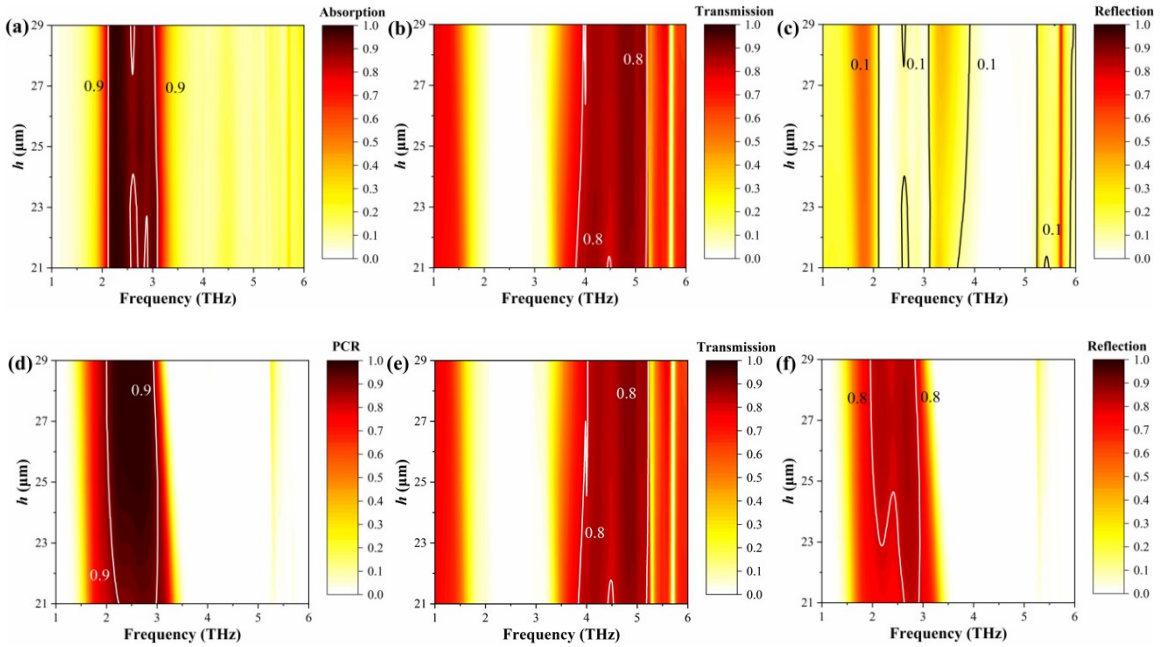

Fig.S3. The effects of the structural parameter *h* on the EM response of the directional AE multifunctional JMS for the forward and backward incident TE waves. (a-c) illustrate the EM responses of the proposed JMS for the forward TE wave versus *h*: a) the absorption versus *h*, b) the co-polarized transmission versus *h*, c) the co-polarized reflection versus *h*. (d-f) show the EM responses of the proposed JMS for the backward TE wave versus *h*: d) the PCR versus *h*, e) the co-polarized transmission versus *h*, f) the cross-polarized reflection versus *h*.

7. Polarization-insensitivity and parameter analysis of JMA

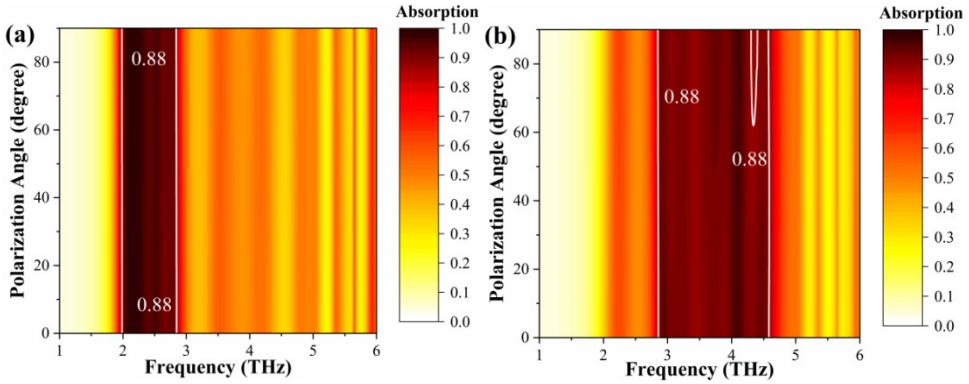

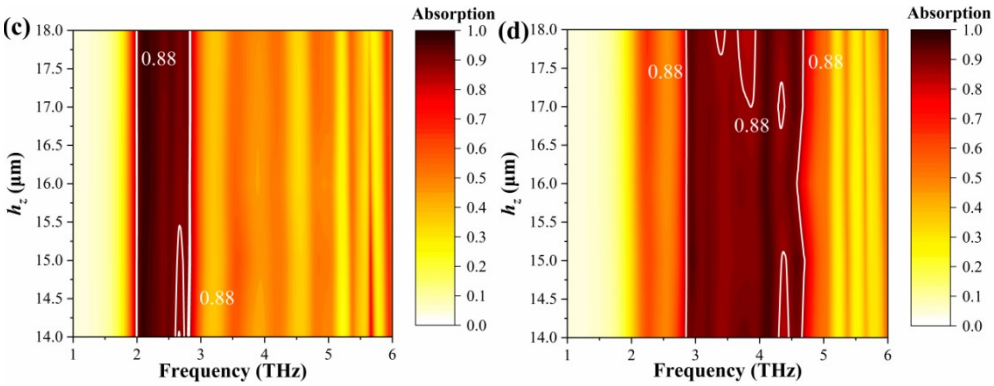

Fig.S4. (a) and (b) illustrate the effects of the polarization angle of the bidirectional normal-incident waves on the absorption of the proposed directional JMA: (a) the forward incident wave, (b) the backward incident wave. (c) and (d) depict the effect of the shifting distance along the *z*-direction h_z on the absorption of the proposed directional JMA for the bidirectional incident TE waves: (c) the forward incident wave, (d) the backward incident wave.

To investigate the effect of the polarization angle of the incident EM wave on the JMA, the EM simulations were performed on its absorption characteristics for the forward and backward vertical-incident waves with different polarization angles, as shown in Figs.S4(a) and (b). As the wave is incident vertically in the forward direction, the absorption efficiency of the JMA always remains stable as the polarization angle increases. Concurrently, the JMA is also insensitive to the variation of polarization angle of the backward normal-incident wave in general, although the absorption efficiency at about 4.35 THz decreases slightly as the polarization angle is above 60°. Therefore, the polarization angle of the bi-directional incident wave has little influence on the absorption characteristic of the designed JMA, which can be attributed to the symmetric configuration. In addition, owing to the significant effect of the coupling between the inner and outer AE cavities on the EM energy harvesting efficiency for the forward and backward incident waves, the action of shifting distance along z-direction hz needs to be investigated, as presented in Figs.S4(c) and (d). With the increase of h_z, the absorption of the JMA for the forward incident TE wave at 2.6 THz is gradually enhanced due to the reduction of the effect of coupling between inner and outer structures on the anapole response existing in the outer elliptical rings. Meanwhile, the impaired coupling also slightly

influences the anapole mode existing in the inner elliptical structure with a small size, thus improving the absorption for the backward incident TE wave at 4.37 THz. However, the absorption for the backward incident TE wave working at 3.2-3.9 THz gradually decreases as the h_z increases. Under the consideration of the absorption efficiency for the bidirectional incident waves, the optimized shifting distance h_z should be chosen as 16 μm.

References

1. E. E. Radescu, and G. Vaman, "Exact Calculation of the Angular Momentum Loss, Recoil Force, and Radiation Intensity for an Arbitrary Source in Terms of Electric, Magnetic, and Toroid Multipoles,"*Phys. Rev. E*, vol. 65, no. 4, pp. 046609, Apr. 2022.
2. V. Savinov, V. A. Fedotov, and N. I. Zheludev, "Toroidal Dipolar Excitation and Macroscopic Electromagnetic Properties of Metamaterials," *Phys. Rev. B,* vol. 89, no.20, pp. 205112, May 2014.
3. G. N. Afanasiev, and Y. P. Stepanovsky, "The Electromagnetic Field of Elementary Time-dependent Toroidal Sources," *J. Phys. A: Gen. Phys.*, vol. 28, no. 16, pp. 4565-4580, Mar. 1995.
4. T. J. Kippenberg, S. M. Spillane, K. J. Vahala, "Fabrication and Coupling to Planar High-Q Silica Disk Microcavities," *Appl. Phys. Lett.*, vol. 85, no. 4, pp. 797-799, May 2003.
5. Y. L. Li, Q. Sun, S. Zu, X. Shi, Y. Q. Liu, X. Y. Hu, K. Ueno, Q. H. Gong, and H. Misawa, "Correlation between Near-Field Enhancement and Dephasing Time in Plasmonic Dimers," *Phys. Rev. Lett.*, vol. 124, no. 16, pp. 163901, Apr. 2020.
6. Y. Xu, Y. Qin, B. Ji, X. Song, J. Lin, "Manipulation of Plasmon Dephasing Time in Nanostructure Arrays Via the Far-field Coupling,"*Plasmonics*, vol. 16, no. 5, pp. 1745-1754, Mar. 2021.